Magnesium Technology 2012
Edited by: Suveen N. Mathaudhu, Wim H. Sillekens, Neale R. Neelameggham, and Norbert Hort
TMS (The Minerals, Metals & Materials Society), 2012

EFFECT OF WELD STRUCTURE ON FATIGUE LIFE OF FRICTION STIR SPOT WELDING IN MAGNESIUM AZ31 ALLOY

H.M. Rao[1], J.B. Jordon[1]
[1]The University of Alabama, Dept. of Mechanical Engineering, Tuscaloosa, AL, 35487, USA

Keywords: Friction stir spot welding, Fatigue, Magnesium alloy

Abstract

In this paper the fatigue behavior in friction stir spot welded coupons of magnesium AZ31 alloy manufactured under different welding conditions are investigated. Two sets of lap-shear coupons were welded based on varying the plunge depth and tool geometry. Metallographic analysis of the untested lap-welds revealed differences in microstructural and geometrical features. Results from the load controlled cyclic tests showed that one set of welds exhibited better fatigue performance compared to the other set. Optical fractography of the failed fatigue coupons revealed that fatigue cracks initiated at the weld interface in both sets of coupons. However, the fracture mode showed variability between the two sets of coupons. As such, the main conclusion of this study is that the effective top sheet thickness, which is largely determined by the shoulder plunge depth, plays a significant role in the fatigue behavior of the friction stir spot welds in magnesium alloys.

Introduction

Friction stir spot welding (FSSW), which is similar to friction stir seam welding, is a thermo-mechanical process for spot lap-joining of sheet metals [1,2]. The rotating tool comprises a probe pin that is plunged into the two sheets of metal to be joined. The probe pin typically penetrates the upper sheet completely and then passes into the bottom sheet to various depths depending on process conditions. Here, the downward force and rotational speed generate localized heat as the pin interacts with the upper sheet. The heat generated by friction softens the two sheets and the softened metal adjacent to the tool deforms plastically and a solid state bond is made between the surface of upper and bottom sheet [3]. Since the dwell time is relatively short, 2 to 5 seconds, the tool rotation speed and plunging motion determine the heat generation [4], joint formation and weld mechanical properties [5]. In general, FSSW is free of many of the defect formation issues commonly associated with fusion welding. This is due to the assumption that, the temperature attained during friction stir welding is less than the melting point of base material. In addition, FSSW is more energy efficient and clean when compared to other types of spot welding. Some of the other advantages include no need of cooling agent, filler materials, or post weld treatment.

As industry continues the push for more fuel-efficient designs, magnesium alloys are receiving increased interest. Thus, FSSW is a favorable technique for spot welding lightweight metals, such as magnesium alloys. Some recent work on FSSW of magnesium AZ31 alloy has focused on process-property-performance relationships [2,5-7]. One of the key findings was related to the size and shape of the interfacial hook. During FSSW, trapped oxide films present between the overlapping sheets are oftentimes displaced in an upward direction toward the top sheet into a "hook-like" shape. This hooking is largely due to the plastic flow of the material resulting from the downward plunge of the pin into the bottom sheet. In fact, higher joint static strengths were found when the hook region was curved more outwards from tool axis and the distance from the hook extremity to the top surface of the weld was the greatest [7]. A similar observation was also found in Al alloys [8]. While fundamental relationships governing the static strength of FSSW in magnesium alloys have been developed, only a few studies exist regarding fatigue [9-10]. In lap-shear fatigue testing, fatigue cracks were found to initiate from this interfacial hook [10]. For cyclic loads approaching the static strength of the joint, the dominant cracks initiated from the interfacial hook and final failure occurred by nugget pullout. However, for lower cyclic loads, fatigue cracks grew from the interfacial hook and then propagated through the top sheet. In this prior study, the height of the interfacial hook was thought to be influential in determining the final number of cycles to failure in magnesium AZ31 alloys.

Beyond the work of Mallick and Agarwal [9], and Jordon et al. [10], the fundamental understanding of fatigue mechanisms in FSSW lap-joints is primarily restricted to aluminum alloys. Lin et al. [11-12] studied fatigue failures in friction spot welded aluminum 6111-T4 sheets, processed using different geometric tools. Under different loading conditions, the failure mode in fatigue was found to vary. In quasi-static loading, it was observed that fatigue cracks initiated from the upper sheet near the stir zone inside the weld. Under cyclic loading conditions, three main types of crack initiations were observed: the first type was similar to quasi-static loading, the second type initiated from stir zone into the bottom sheet and the third initiated from the bend in the upper sheet. In addition, Lin et al. [11] compared the failure modes of FSSW made using different tool geometries. Spot welds created using a flat tool initiated cracks from several locations compared to a concave tool. The amount of material deformation during the welding process due to the shape of the tooling was identified as the likely reason for the difference in failure modes of the flat and concave tooling. The fatigue cracks were observed to initiate near the possible original hook tip in the stir zone and propagated along the circumference of the nugget, then through the sheet thickness and finally along the width of the specimen [3].

To best of authors' knowledge, the effect of weld structure due to variation in welding conditions on fatigue has not been established for magnesium alloys. In this paper, fatigue performance and failure mechanisms of the FSSW magnesium AZ31 alloy coupons manufactured under different process conditions has been studied. Furthermore, we attempt to establish cause and effect relationships for fatigue in FSSW with respect to microstructural and geometrical features.

Material and Experiments

Magnesium AZ31 alloy sheets of 2.0 mm thickness were chosen for the present study. Two sets of FSSW coupons were welded in

an overlap configuration. For process #1, the individual sheet dimensions were: length of 100 mm, width of 35 mm, and a welded overlap area of 35 X 35 mm. For process #2, the individual sheet dimensions were: length of 100 mm, width of 38 mm and a welded overlap area of 38 X 38 mm. For process #1, the FSSW tool was made from standard tool steel (H13) material, having a shoulder with a diameter 12 mm, pin length of 3.2 mm and left hand threads (M5) as shown in Fig. 1a. For process #2, the FSSW tool is identical to the tool used in process #1; however the tool had a triangular pin as shown in Fig. 1b. Both tools had a 10-degree concave shoulder as shown in Fig. 1c. Table I lists the welding process conditions used to join the two sets of lap-shear coupons employed in this study. Figure 2 shows representative samples from both process #1 and #2.

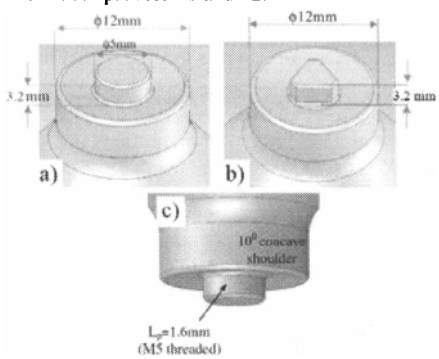

Figure 1. Schematic of the FSSW tool geometry employed for (a) process #1 and (b) process #2 [8]. The tool for process #1 had a cylindrical pin with a diameter of 5 mm and M5 threads. The tool for process #2 had a triangular pin. Both tools had a (c) concave shoulder of 10 degrees and a diameter of 12 mm with a pin length of 1.6 mm.

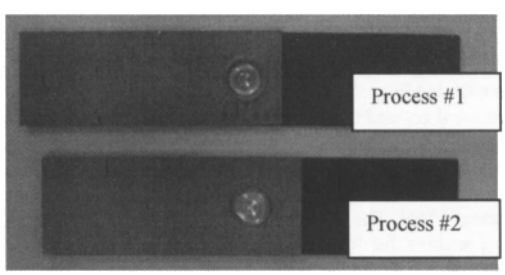

Figure 2. Representative lap-shear coupons produced from process #1 and process #2.

Table I: Friction stir spot welding conditions.

Welding Parameters	Process #1	Process #2
Tool rotation (RPM)	1000	750
Tool Plunge Speed (mm/min)	20	20
Shoulder Plunge Depth (mm)	0.5	0.1
Dwell Time (sec)	2.5	2.5

For the fatigue tests, the lap-shear coupons were cyclically tested in an MTS 810 servo-hydraulic load frame under load control with a sinusoidal waveform at three different load ratios (0.1, 0.3, and 0.7). The fatigue tests were tested at frequencies that ranged from 5–30 Hz. While most of the tests were conducted at 10 Hz, higher frequencies were employed for the low load amplitudes to expedite failure. Steel shims were employed in the test frame to prevent the addition of bending forces. The grip-to-grip distance employed for each coupon was 110 mm. For weld characterization, samples were sectioned through the center of the weld nugget coupon and parallel to the loading direction. Samples were cold mounted in epoxy and mechanically ground and polished. Using a Keyence VHX-1000 digital optical microscope, key features of the weld were quantified including size and shape of the interfacial hook, the bond width, and distance from the shoulder of the nugget to the root of interfacial hook. In order to reveal the microstructure of the FSSW coupons, the samples were etched using a 4.2 g picric acid, 10 ml acetic acid, 10 ml H2O, and 70 ml ethanol [13]. Typical optical micrographs of the stir zone, thermomechanically affected zone (TMAZ), and the heat-affected zone (HAZ) were obtained. Representative failed coupons from process #1 and process #2 were also observed under the Keyence microscope to study the crack propagation and failure modes under different loading conditions. In addition, fracture surfaces of failed fatigue coupons were examined under a Jeol 7000 scanning electron microscope with the intent to estimate the fatigue crack growth rate.

Results

Microstructure

Representative microstructure images of coupons from process #1 and process #2 are shown in Fig 3. Overall, the grains were similar in size in both processes. In particular the average grain size in the stir zone, which comprised recrystallized grains, was approximately 9 μm in both processes. Elongated grains were observed in the TMAZ and partially recrystallized grains were observed in the HAZ.

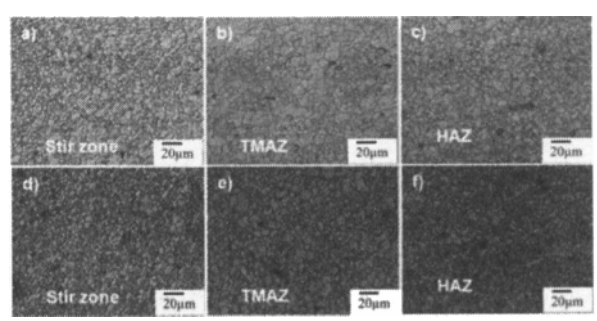

Figure 3. Microstructure features showing: (a) stir zone, (b) TMAZ, (c) and HAZ in coupons from process #1, and (d) stir zone (e), TMAZ, (f) and HAZ in coupons from the process #2.

Interfacial Hooking and Geometrical Features

Figure 4 shows magnified views of the interfacial hook in process #1 (4a) and process #2 (4b). For clarification purposes, we label the two peaks of the interfacial hook as primary and secondary as noted in Fig. 4. In both processes, primary and secondary hooks were observed. Moreover, process #2 produced a smoother interface and more well defined hooking. In contrast, the interfacial hook exhibited a more erratic path in process #1 and the distinction between the primary and secondary hook was not as clear as in process #2. Lastly, the height of the hooks varied greatly between both processes, where in process #2 the hook heights were approximately three times as large as compared to process #1. This large difference in hook height between the two

processes is likely due the difference in tool plunge depth. However, additional experiments are needed to confirm this.

In addition, the sheet thicknesses in the weld nugget were measured, where for process #2, the top sheet thickness in the weld nugget was almost identical to the nominal thickness of the magnesium alloy sheets (2 mm). However, process #1 had an effective sheet thickness in the weld nugget of 1.3 mm. As such, the link between this effective sheet thickness is directly related to the shoulder plunge depth during welding. In process #2, the shoulder plunge depth was 0.1 mm, compared to 0.5 mm for process #1. As such, the deeper the shoulder of the tool is plunged, the smaller the thickness of the sheet in the weld zone. Lastly, the bond widths of the welds were similar in size for both processes.

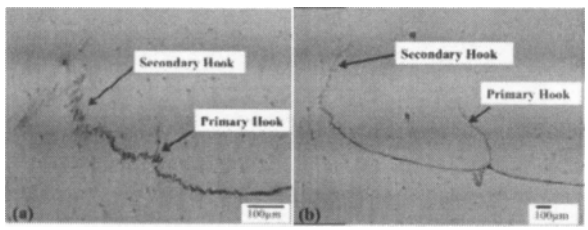

Figure 4. Magnified views of the primary and secondary hooks formed in (a) process #1 and (b) process #2.

Cyclic Testing

Figure 5 shows the results of the fatigue tests for both processes. In general, the fatigue lifetimes associated with final separation were greater for process #2 when compared to process #1. The results also show that the FSSW lap-joint did not exhibit a load ratio effect commonly found in uniaxial base material experiments [cf. 14].

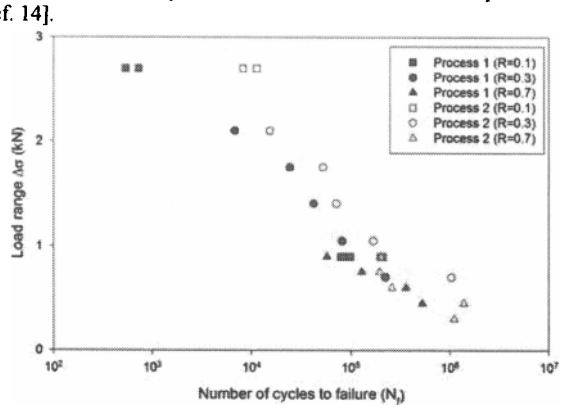

Figure 5. Experimental results of the load range versus the number cycles to failure for complete separation for friction stir spot weld lap-shear coupons tested at three load ratios (R=0.1, 0.3, 0.7).

Fractography

Figure 6 shows an overview of representative fractured coupons from both process #1 and #2. Several macroscale observations were made regarding the failure modes. For the coupons from the process #1 and #2 tested at a maximum cyclic load of 2 kN or greater, fracture of the weld occurred by failure of the weld nugget. Below 2 kN, the joints failed by fatigue crack propagation through the sheet thickness. For process #1, the dominant crack grew from the primary hook towards the top surface of the top sheet and then propagated along the outer circumference of the nugget. Halfway around the nugget circumference, the crack grew along the width of the top sheet and failed by top sheet pullout. This failure mode was similar to failure modes observed in aluminum FSSW [3]. As shown in Fig. 7a, the nugget was seen intact in the remaining top and bottom sheet. Figure 7b shows the location of where the primary crack initiated on the outer surface of the weld. It is evident from Fig. 7c that the dominant crack propagated from the faying surface. Higher magnification of the interfacial hook region showed that the primary hook propagated towards the surface of the top sheet. Also evident was that the dominant crack initiated and propagated from the primary hook as shown in Fig. 7d. No evidence of a secondary crack was found elsewhere as shown in the magnified view of Fig 7e, which is located at the opposite side of the weld (180 degrees around the circumference).

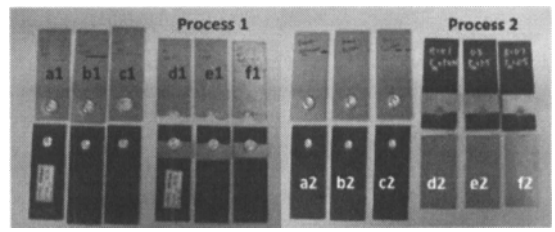

Figure 6. Representative fractured coupons tested at a range of maximum cyclic loads of 1-3 kN at R=0.1, 0.3, and 0.7 (Refer to Table II for a summary of failure modes).

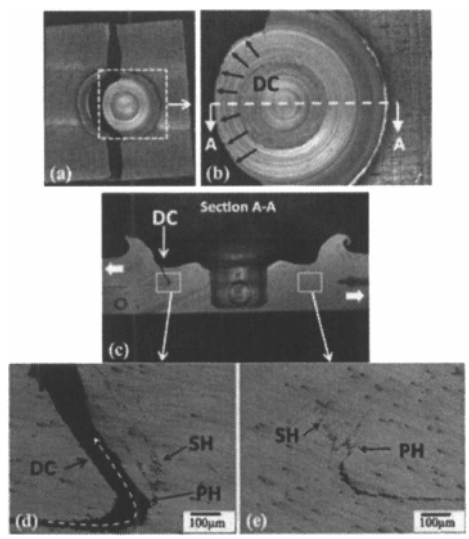

Figure 7. Crack propagation and failure mechanisms for process #1 coupon loaded at a maximum cyclic load of 1 kN at R=0.3. (a) An overview of the surface of the top sheet and (b) a magnified view of the location of surface crack initiation. (c) A section view of the weld nugget shows that the dominant crack (DC) propagated from the weld interface, and (d) and (e) show higher magnification images of the interfacial primary (PH) and the secondary (SH) hooks. Bold arrows in (c) indicate direction of applied loading.

At higher loads in process #1, differences in the failure mode were observed. Coupons tested at and above a maximum cyclic load of 2.5 kN failed by nugget pullout. The dominant crack grew from the primary hook towards the top sheet along the outer circumference of the nugget and failed by nugget pullout as shown in Fig. 8a and 8b. The cross-section view of the weld nugget revealed cracks propagated from the interfacial hooks as shown in Fig. 8c. As shown in Fig. 8d, the dominant crack grew from the primary hook (PH) to the top sheet and secondary cracks (SC) were observed to propagate partially into the bottom sheet as shown in Figure 8e. However, these secondary cracks were not the dominant cracks and did not contribute to final failure. These cracks either propagated at a significantly lower rate, or as the dominant crack became larger it shielded the secondary crack such that they arrested.

Coupons from process #2 tested below a maximum cyclic load of 2.5 kN failed by bottom sheet failure as shown in Fig. 9a. As shown in Fig. 9b, secondary non-dominant cracks were observed to initiate to the top sheet, but did not contribute to the final separation of the coupon. A section view of the nugget confirmed that the dominant crack propagated into the bottom sheet as shown in Fig. 9c. Magnified views of the interfacial hooks shown in Fig. 9d confirmed that secondary cracks (SC) on the opposite side of the nugget propagated to the top sheet from both primary and secondary hooks. However, these cracks did not contribute to the final failure. As shown in Fig. 9d, the dominant crack (DC) grew from the root of the secondary hook towards the bottom sheet and then across the full width of the bottom sheet.

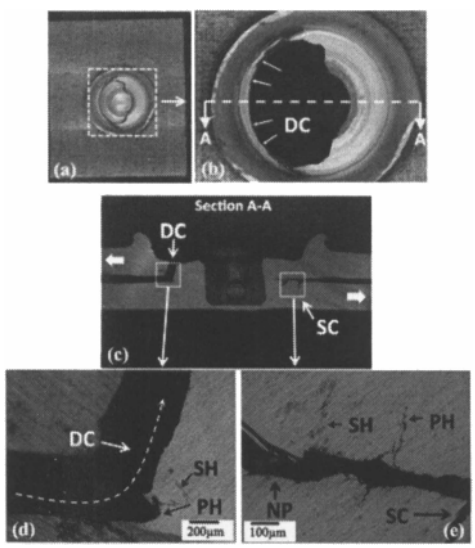

Figure 8. Crack propagation and failure mechanisms for process #1 coupon loaded at a maximum cyclic load of 3 kN at R=0.3. An overview image of the (a) surface of the top sheet and (b) a magnified view of the location of surface crack initiation. (c) A section view of the weld nugget shows that the dominant crack (DC) propagated from the weld interface, and (d) and (e) show higher magnification images of the interfacial primary (PH) and the secondary (SH) hooks. Bold arrows in (c) indicate direction of applied loading.

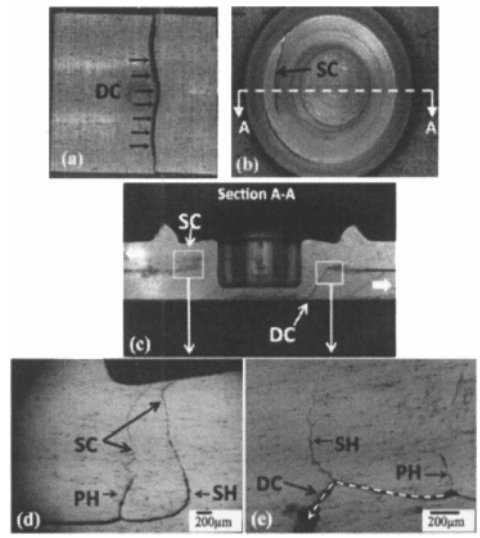

Figure 9. Crack propagation and failure mechanisms for process #2 coupon loaded at a maximum cyclic load of 1 kN at R=0.3. An overview image of the (a) surface of the bottom sheet showing the dominant crack and (b) top sheet showing a secondary crack. (c) A section view of the weld nugget shows that the dominant crack (DC) propagated downward into the bottom sheet and (d) and (e) show higher magnification images of the interfacial primary (PH) and the secondary (SH) hooks. Bold arrows in (c) indicate direction of applied loading.

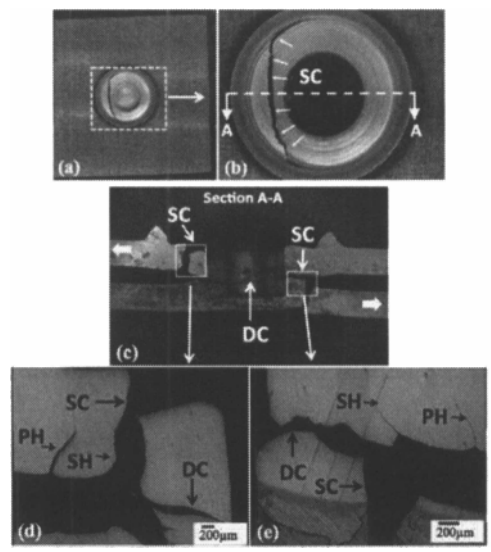

Figure 10. Crack propagation and failure mechanisms for process #2 coupon loaded at a maximum cyclic load of 3 kN at R=0.3. An overview image of the (a) surface of the top sheet and (b) a magnified view of the location of surface crack initiation of the secondary crack (SC). (c) A section view of the weld nugget shows that the dominant crack (DC) was primarily a mode II crack resulting in shear failure, and (d) and (e) show higher magnification images of the interfacial primary (PH) and the secondary (SH) hooking regions. Bold arrows in (c) indicate direction of applied loading.

Coupons from process #2 tested at a maximum cyclic load of 2.5-3 kN failed by interfacial shear failure. Figure 10a shows the top surface of the process #2 coupon tested at 3 kN at R=0.3. It is important to note that the top of the weld nugget remained intact and that a secondary crack was observed to penetrate the top surface of the nugget as shown in Fig 10b. However, this was not the dominant crack. The section view of the nugget region shows evidence of multisite cracking; however the dominant crack grew parallel to the loading direction in mode II as shown in Fig. 10c. Figure 10d and 10e show magnified views of the hooking regions, which indicate that secondary cracks (SC) grew through the primary and secondary hooks. Also shown in Fig. 10e is that secondary cracks were observed to propagate into the bottom sheet. Table II summarizes the fracture modes for the FSSW Mg AZ31 coupons subjected to cyclic loading for both process #1 and #2 based on the optical fractography conducted in this study.

Table II: Summary of failure modes in coupons of process #1 and process #2 (ID correlates with specimens shown in Fig. 6).

ID	Load Ratio (R)	Max Load (kN)	Mode of Failure
Process #1			
a1	0.1	3	Dominant crack grew from primary hook into the top sheet, then halfway around the outer circumference of the nugget, finally failing by nugget pullout.
b1	0.3	2.5	
c1	0.7	3	
d1	0.1	1	Dominant crack grew from primary hook into the top sheet, halfway around the outer nugget circumference and then along the width of the top sheet.
e1	0.3	1.5	
f1	0.7	1	
Process #2			
a2	0.1	3	Dominant crack grew across the weld nugget and parallel to loading direction in mode II propagation.
b2	0.3	3	
c2	0.7	3	
d2	0.1	1	The Dominant crack grew from root of the secondary hook into the bottom sheet, propagated around the outer circumference of the nugget region and then along the width of the bottom sheet.
e2	0.3	1.5	
f2	0.7	2.5	

SEM Analysis

In order to confirm crack failure modes and to estimate crack growth rates in both sets of coupons, representative fracture surfaces of the dominant cracks were imaged using an SEM under high magnification with the intent to measure striation spacing. As shown in Figure 11a, the striation spacing was in the range of 1-1.6 μm for the process #1 coupons testing at a maximum cyclic load of 1 kN. At higher loads, the striation spacing was observed to be in the 3.3-3.5 μm range, as shown in Fig. 11b. In coupons from process #2 tested at a maximum cyclic load of 1 kN, the average striation spacing was around 0.80 μm and in coupons tested at 3kN, the striation spacing was approximately 0.60 μm. We note that the difference between the 1 kN and 3 kN for process #2 is small and this observed difference could also be due to scatter. We also note that the striations were less distinct in process #2 and as such, were considerably more difficult to find compared to process #1.

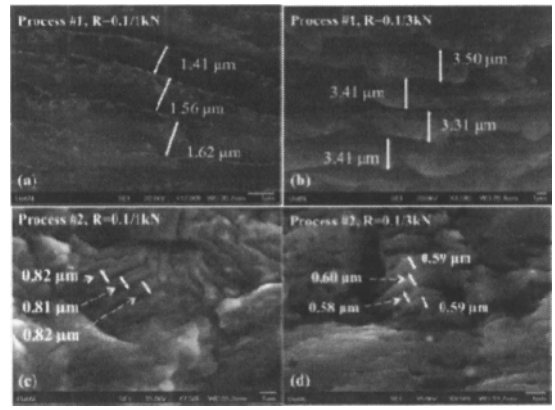

Figure 11. Scanning electron microscope images of striation spacing for: (a) process #1 coupons tested at maximum cyclic load of 1 kN, (b) process #1 coupons tested at maximum cyclic load of 3 kN, (c) process #2 coupons tested at maximum cyclic load of 1 kN, and (d) process #2 coupons tested at maximum cyclic load of 3 kN. Each of these coupons were tested at R=0.3.

Discussion

Analysis of the fractography results presented in the previous sections give an understanding of the underlining mechanisms of fatigue damage in FSSW lap-shear joints of various welding parameters. First, it is worth noting that Yin et al. [7] found that the monotonic strength of FSSW Mg AZ31 coupons increased when the bonded width is large, the distance from the hook extremity to the top surface of the weld was the greatest, and if the hook region is curved outward from the axis of rotating tool. In this study, the main difference between the two processes is related to the effective sheet thickness and the height of the hook, where the distance from the hook extremity was greatest in process #2. As such, it appears that Yin et al. [7] conclusions may be also true for fatigue performance. However, in lieu of establishing an empirical relationship between geometrical and microstructural features to fatigue performance as a way to explain the differences in two set of welds, we focus on the mechanics of fatigue crack damage. As such, the concepts of linear elastic fracture mechanics provide the basis for this discussion. If the spot weld is analyzed in terms of a stress intensity factor, we would expect process #2 to exhibit better fatigue resistance since the effective top sheet thickness was considerably larger in process #2 (2 mm) when compared to process #1 (1.2 mm). In the lap-joint configuration, the effective top sheet thickness largely determines the global stress field, which in turn affects the driving force behind crack initiation and crack growth. When we consider process #1, the smaller effective top sheet thickness would likely produce a higher stress intensity factor which would drive the dominant crack to propagate through interfacial hook. As shown in Fig. 7-8, the experimental results do indeed show that the dominant crack initiated and grew through the interfacial hooks for process #1 over the full range of low cyclic loads testing in this study. Likewise, in process #2, it is the effective top sheet thickness that again determines the facture mode. The stress intensity factor would likely be lower in process #2 due to the significantly thicker top sheet thickness. This lower stress intensity would reduce the driving force for dominant mode I crack growth through the top sheet and allow for an alternant location of crack initiation and crack growth. This

was confirmed experimentally, where at the higher maximum cyclic loads, the dominant crack was observed to be a predominantly mode II type crack, which resulted in better fatigue lifetimes. At lower maximum cyclic loads, the initial cycles likely do not fully open the interfacial hook, which would further repress the stress intensity factor and allow for the dominant crack to propagate through the bottom sheet as was observed experimentally and shown in Fig. 10.

Lastly, we note that the SEM images of the fracture surface suggest that the cracks propagated at a higher rate in process #1 compared to process #2. This supports the hypothesis that the effective top sheet thickness is the dominant factor controlling fatigue performance in FSSW. In fact, based on the analysis of the experimental results presented here, one can conclude that the better fatigue performance of process #2 is largely determined by the tooling and welding conditions which, in turn, affected the structural integrity of the weld.

Conclusions

In this study, the influence of microstructural and geometrical features on fatigue lifetimes are evaluated on two different sets of friction stir spot welded lap-shear coupons. Several differences in the initial state of the weld structure including size and shape of the interfacial hooks and the effective top sheet thickness were observed between the two processes. Fractography analysis conducted in this study suggested that the effective top sheet thickness largely determined the failure mode, which in turn influenced the final number of cycles to failure. While the height of the interfacial hook was greater in the process with better fatigue performance, it was the larger effective top sheet thickness that promoted crack propagation modes more favorable to greater fatigue resistance. As such, the shoulder plunge depth during the friction stir welding process may likely be the dominant factor in producing durable spot welds using this novel welding technique.

Acknowledgements

The authors would like to recognize Mark Horstemeyer, Jim Quinn, Joy Forsmark, Xuming Su, Alan Luo, Robert McCune, AK Khosrovaneh, and Lin Zhang for their encouragement of this study. The authors would also like to thank Harsha Badarinarayan for providing the FSSW coupons. In addition, the authors would like to thank Jenna Grantham for conducting the fatigue tests. This material is based upon work supported by the Department of Energy National Energy Technology Laboratory under Award Numbers DE-FC26-02OR22910 and DE-EE0003583. This work was prepared as an account of work sponsored by an agency of the United States Government. Neither the United States Government nor any agency thereof, nor any of their employees, makes any warranty, express or implied, or assumes any legal liability or responsibility for the accuracy, completeness, or usefulness of any information, apparatus, product, or process disclosed, or represents that its use would not infringe privately owned rights. Reference herein to any specific commercial product, process, or service by trade name, trademark, manufacturer, or otherwise does not necessarily constitute or imply its endorsement, recommendation, or favoring by the United States Government or any agency thereof. The views and opinions of authors expressed herein do not necessarily state or reflect those of the United States Government or any agency thereof.

References

1. S.M. Chowdhurya, D.L. Chena, S.D. Bholea, and X. Caob, "Tensile Properties of a Friction Stir Welded Magnesium Alloy: Effect of Pin Tool Thread Orientation and Weld Pitch," *Materials Science and Engineering A*, 527 (2010), 6064–6075.

2. Y.H. Yin, N. Sunb, T.H. North, and S.S. Hua, "Hook Formation and Mechanical Properties in AZ31 Friction Stir Spot Welds," *Journal of Materials Processing Technology*, 210 (2010), 2062–2070.

3. D.A. Wang, and C.H. Chen, "Fatigue Lives of Friction Stir Spot Welds in Aluminum 6061-T6 Sheets," *Journal of Materials Processing Technology*, 209 (2009), 367-375.

4. A. Gerlich, P. Su, and T.H. North, "Tool Penetration During Friction Stir Spot Welding of Al and Mg Alloys." *Journal of Materials Science*, 40 (2005), 6473–6481.

5. Y.H. Yin, A. Ikuta, and T.H. North, "Microstructural Features and Mechanical Properties of AM60 and AZ31 Friction Stir Spot Welds," *Materials and Design*, 31 (2010), 4764–4776.

6. N. Sun, Y.H. Yin, A.P. Gerlich, and T.H. North, "Tool Design and Stir Zone Grain Size in AZ31 Friction Stir Spot Welds," *Science and Technology of Welding and Joining*, 14 (2009), 747-752.

7. Y.H. Yin, N. Sun, T.H. North, and S.S. Hu, "Influence of Tool Design on Mechanical Properties of AZ31 Friction Stir Spot Welds," *Science and Technology of Welding and Joining*, 15 (2010), 81-86.

8. H. Badarinarayan, Y. Shi, X. Li, X, and K. Okamoto, "Effect of Tool Geometry on Hook Formation and Static Strength of Friction Stir Spot Welded Aluminum 5754-O Sheets," *International Journal of Machine Tools and Manufacture*, 49 (2009), 814–823.

9. P.K. Mallick, and L. Agarwal, "Fatigue of Spot Friction Welded Joints of Mg-Mg, Al-Al and Al-Mg Alloys," (Paper presented at Society of Automotive Engineers, Warrendale, PA, 2009) 2009-01-0024.

10. J.B. Jordon, M.F. Horstemeyer, S.R. Daniewicz, H. Badarinarayan, and J. Grantham, "Fatigue Characterization and Modeling of Friction Stir Spot Welds in Magnesium AZ31 Alloy," *Journal of Engineering Materials and Technology*, 132 (2010), 041008-1-10.

11. P.C. Lin, J. Pan, and T. Pan, "Failure Modes and Fatigue Life Estimations of Spot Friction Welds in Lap-Shear Specimens of Aluminum 6111-T4 Sheets. Part 1: Welds Made by a Flat Tool," *International Journal of Fatigue*, 30 (2008), 74-89.

12. P.C. Lin, J. Pan, and T. Pan, "Failure Modes and Fatigue Life Estimations of Spot Friction Welds in Lap-Shear Specimens of Aluminum 6111-T4 Sheets. Part 2: Welds Made by a Flat Tool," *International Journal of Fatigue*, 30 (2008), 90–105.

13. N. Afrin, D.N. Chen, X. Cao, and M. Jahazi, "Microstructure and Tensile Properties of Friction Stir Welded AZ31B Magnesium Alloy," *Materials Science and Engineering A*, 427 (2008), 179–186.

14. S. Suresh, *Fatigue of Materials* (United Kingdom: Cambridge University Press, 1998), 204.